International Journal of Coal Science & Technology (2024) 11:31
https://doi.org/10.1007/s40789-024-00686-w

RESEARCH

Understanding poromechanical response of a biogenic coalbed methane reservoir

Rohit Pandey[1] · **Satya Harpalani**[2]

Received: 23 September 2023 / Revised: 17 November 2023 / Accepted: 14 March 2024
© The Author(s) 2024

Abstract
Biogenic coalbed methane (BCBM) reservoirs aim to produce methane from in situ coal deposits following microbial conversion of coal. Success of BCBM reservoirs requires economic methane production within an acceptable timeframe. The work reported here quantifies the findings of previously published qualitative work, where it was found that bioconversion induces strains in the pore, matrix and bulk scales. Using imaging and dynamic strain monitoring techniques, the bioconversion induced strain is quantified here. To understand the effect of these strains from a reservoir geomechanics perspective, a corresponding poromechanical model is developed. Furthermore, findings of imaging experiments are validated using core-flooding flow experiments. Finally, expected field-scale behavior of the permeability response of a BCBM operation is modeled and analyzed. The results of the study indicated that, for Illinois coals, bioconversion induced strains result in a decrease in fracture porosity, resulting in a detrimental permeability drop in excess of 60% during bioconversion, which festers itself exponentially throughout its producing life. Results indicate that reservoirs with high initial permeability that will support higher Darcian flowrates, would be better suited for coal bioconversion, thereby providing a site-selection criteria for BCBM operations.

Keywords Coal bioconversion · Poromechanical model · Reservoir response · Bioconversion induced strain

1 Introduction and background

Methane, naturally occurring in coal seams due to thermogenic (high temperature and pressure) and biogenic (microbial) effects, has been extracted economically in the US since the late eighties. Microbially enhanced coalbed methane (MECBM), first introduced by Andrew Scott in 1999 (Scott 1999), aims to replicate the natural process of biogenic methane formation in situ. Given the environmental benefits of burning natural gas for electricity generation, microbial conversion of coal to methane has attracted significant attention in the recent past (Fallgren et al. 2013; Opara et al. 2012; Strapoc et al. 2007, 2008; Wei et al. 2014; Zhang et al. 2016a, b). A MECBM reservoir requires treating in situ coal with nutritionally-amended microbial solutions, and allowing it to produce biogenic methane over the treatment duration. Post-treatment, the MECBM reservoir behavior is expected to be similar to traditional CBM reservoirs. The producing life of a traditional CBM reservoir is typically between ten to twenty years, although few CBM wells have been producing for close to three decades. Thus, there are currently several depleted/near-depletion CBM wells in the mature basins, such as, San Juan and Black Warrior, with surface infrastructure in place that can be used for microbial re-charge and production (Wawrik et al. 2012).

Since its inception, the major research focus towards bioconversion of coal has been from a microbial perspective. Experimental studies presented by multiple researchers (Opara et al. 2012; Strapoc et al. 2007; Zhang & Liang 2017) have reported biogenic methane generation rates, often in excess of 500 standard cubic feet per ton of coal (scft), from different coal types. A few studies have also reported generation rates in excess of 2000 scft (Zhang et al. 2018a, b). Subsequent insight into the economics of biogenic methane production has been reported as well (Zhang et al. 2016a, b). However, production from a biogenically recharged CBM reservoir, referred to as a BCBM reservoir, requires characterization of fluid transport behavior of treated coals. Given

✉ Rohit Pandey
rpandey@vt.edu

[1] Virginia Tech, Blacksburg, USA

[2] Southern Illinois University, Carbondale, USA

Published online: 17 April 2024

that coal serves the role of the source as well as reservoir rock for the produced methane, reservoir implications of bioconversion are important from a feasibility perspective. The reservoir response, particularly for coal reservoirs, is multi-faceted, requiring extensive characterization, which will be one of the focus areas of the work presented here.

Flow in a traditional CBM reservoir is governed by the physical structure of coal, characterized as a dual-porosity rock, where the micro- and macro- porosities affect the transport of fluids through it. Micropores occur as a part of the coal matrix and serve as a storehouse for over 95% of the gas in adsorbed form (Gray 1987). The macropore system consists of a network of closely placed natural fractures surrounding the matrix blocks, known as the cleat system. The dual-porosity structure of coal dictates the transport of fluids in the reservoir. Over the course of CBM production, say in the San Juan basin, where coal is completely water saturated, pumping out water reduces the pore pressure, resulting in desorption of methane from the microporous matrix surface, contributing to the first stage of fluid transport in coal. Once desorbed, methane diffuses across the complex pore geometry of coal in accordance with Fick's second law of diffusion. Methane then reaches the cleat system, where the transport mechanism becomes Darcian, characterized by its permeability. The cleat permeability is dependent on cleat parameters, like aperture, continuity and spacing. Characterizing the fluid-flow behavior and related reservoir characterization are, therefore, critical to assess the economic viability of CBM and potential BCBM reservoirs. However, there is a dearth of studies on evaluation of the impact of bioconversion induced changes on reservoir characteristics. Experimental work conducted on powdered coal to characterize changes in sorption properties as a result of bioconversion was first reported by Pandey et al. (2016), and then by Zhang et al. (2017). It was reported that increase in microporous surface area post-bioconversion results in increased sorption capacity of coal. Bioconversion also resulted in increased diffusion rates for methane and carbon dioxide (Pandey et al. 2016). Such variations translate to increased microporous surface area available for sorption and altered pore geometry, resulting in increased flowrates (diffusive) at the microscopic scale. Increased porosity of coal post-bioconversion was also evident in the images presented by Zhang et al. (2018a, b), where ~ 5000 scft of methane was produced over the year-long treatment duration. Figure 1, adapted from the aforementioned study, presents an image showing increased matrix porosity and polymer deposition post-bioconversion. Alteration in microporosity has also been recently reported for the Jurassic Yanan formation (Li et al. 2023), where the connecting bonds of coal aromatic layers are destroyed and the distance between the aromatic layers reportedly get larger.

Another distinctive feature of CBM reservoirs, setting it apart from traditional natural gas reservoirs, is the competing mechanisms of poromechanical cleat compression and desorption-induced matrix shrinkage. Removal of water to initiate gas production results in reduction in pore pressure, thereby increasing the horizontal effective stress (defined as the difference between the in situ horizontal stress and pore pressure). The existing pore pressure that keeps the cleat apertures open starts to decrease, thus closing the cleats and decreasing the permeability and flowrates. On the other hand, as methane desorbs from the microporous coal surface, it results in shrinkage of the coal matrix which, in turn, widens the cleat/fracture apertures in coal, thereby boosting gas production. The shrinkage effect competes with the

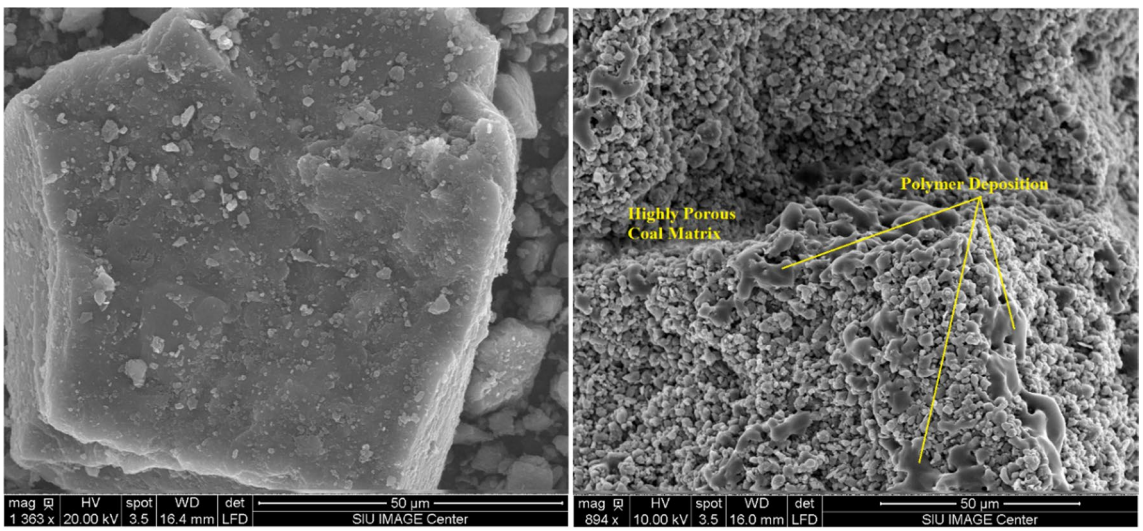

Fig. 1 Illinois coal before and after year-long microbial treatment. (adapted from Zhang et al 2018a, b, 2018a)

mechanical effect of the change in effective horizontal stress, thereby dictating the permeability variation with depletion in CBM reservoirs. Several stress and permeability models, which capture these two effects and describe the flow behavior in CBM reservoirs, have been presented over the years. Gray (1987) proposed the first model using a stress-based approach in 1987. Following this, multiple models (Connell et al. 2010; Cui and Bustin 2005; Harpalani and Chen 1997; Palmer and Mansoori 1998; R 1996; Sawyer et al. 1990; Shi and Durucan 2004) were presented for various boundary conditions governing the flow in CBM reservoirs. All models primarily capture the changes in fracture geometry over the life of a producing reservoir which, in turn, dictates the reservoir flow behavior.

Previously reported work (Pandey and Harpalani 2018) captured the effect of bioconversion on the fracture geometry of coal. The results indicated that, post-bioconversion, there is a considerable change in the fracture/cleat aperture size of coal. They further pointed out that bioconversion generally resulted in reduction of the cleat aperture by ~ 95% of the observed instances for fractures < 5 μm in aperture. However, the aperture size increased post-bioconversion for fractures with apertures larger than ~ 5 μm in width. Such varied effects of bioconversion on cleat apertures would result in a variation in the expected flowrates from the reservoir. However, only a qualitative description of this effect on reservoir properties was provided in the previously reported work (Pandey and Harpalani 2018), necessitating the need for quantitative understanding of the strains developed in the coal fracture, matrix and bulk due to bioconversion.

Quantification of both matrix and fracture-pore strains is critical to understand the effect of bioconversion on the flow-governing structural properties of coal. In the work presented here, we first quantify the fracture-pore strains developed in coal due to bioconversion, using images obtained and reported previously (Pandey and Harpalani 2018). The fracture-pore strains referred here onwards refer to the cleat/fracture porosity, and not microporosity. However, imaging techniques do not allow accurate measurement of matrix strain developed as a result of bioconversion. Hence, in a novel experiment designed, coal matrix strain was measured continuously while samples were undergoing bioconversion. In a parallel effort, a poroelastic model was developed which modifies the existing governing equation for flow-coupled-geomechanics of CBM reservoirs to account for the bioconversion induced strains. The modified equation was then used to understand the variation in the state of effective stress and pressure-dependent-permeability (*pdk*) response of a BCBM reservoir. The trends predicted by imaging results were correlated with variations in laboratory measured permeability due to bioconversion, as reported in two separate studies (Pandey and Harpalani 2019c; Stephen et al. 2014). Finally, field-scale modeling of a BCBM operation from a permeability perspective was carried out to improve our understanding of the expected reservoir response to biogenic recharge and production.

2 Model development

In this section, an effective stress model describing flow-coupled geomechanical behavior of BCBM reservoirs is derived from the constitutive poroelastic equations for a homogenous, isotropic, thermoelastic porous medium. The expression is given as (Bear and Corapcioglu 1981; Nowacki 1970):

$$\widetilde{\sigma}_{ij} = 2G\widetilde{\epsilon}_{ij} + \lambda\widetilde{\epsilon}\delta_{ij} + K\alpha_T\widetilde{T}\delta_{ij} \tag{1}$$

where, δ_{ij} is the Kronecker delta, σ is the effective stress,ϵ is the volumetric strain, G is the shear modulus, λ is the Lame's constant, K is the bulk modulus of the porous media, α_T is the coefficient of volumetric thermal expansion and T is the temperature of the media. The ˜ sign indicates incremental values of these parameters. Also, the volumetric strain ϵ can be represented by the sum of the strains in the X (ϵ_{xx}), Y (ϵ_{yy}) and Z (ϵ_{zz}) directions where, $\widetilde{\epsilon} = \widetilde{\epsilon}_{xx} + \widetilde{\epsilon}_{yy} + \widetilde{\epsilon}_{zz}$, and effective stress increment ($\widetilde{\sigma}_{ij}$) is expressed as $\widetilde{\tau}_{ij} = \widetilde{\sigma}_{ij} + \widetilde{p}\delta_{ij}$, where $\widetilde{\tau}_{ij}$ is the total stress increment and p is the pore pressure.

The coal fabric is known to shrink/swell with methane desorption/adsorption. The sorption-induced matrix strains are assumed to be directly analogous to thermal strains developed in the fabric due to changes in temperature. The most widely used models characterizing effective stress and *pdk* response of CBM reservoir depletion have successfully modeled laboratory and field scale observations using this assumption (Palmer and Mansoori 1998; Shi and Durucan 2005). Equation (1) is thus rewritten as:

$$\widetilde{\sigma}_{ij} = 2G\widetilde{\epsilon}_{ij} + \lambda\widetilde{\epsilon}\delta_{ij} + K\widetilde{\epsilon}_{\mathrm{S}}\delta_{ij} \tag{2}$$

The sorptive strain, ϵ_{S} at any pore pressure p, is described using the Langmuir-type model, characterized using the Langmuir-type parameters, maximum strain (ϵ_{l}) and pressure (p_{ϵ}):

$$\epsilon_{\mathrm{S}} = \frac{\epsilon_{\mathrm{l}} p}{p + p_{\epsilon}} \tag{3}$$

The strain developed due to bioconversion, expressed by $\widetilde{\epsilon}_T$, is the primary focus of the work presented, is also assumed to be analogous to thermal strains. Hence, the constitutive expression describing the effective stress for bioconverted coalbed methane reservoirs is written as:

$$\widetilde{\sigma}_{ij} = 2G\widetilde{\epsilon}_{ij} + \lambda\widetilde{\epsilon}\delta_{ij} + K\widetilde{\epsilon}_{\mathrm{S}}\delta_{ij} + \varkappa\widetilde{\epsilon}_T\delta_{ij} \tag{4}$$

where, $\varkappa$ is the modulus of the reservoir undergoing bioconversion. Such a distinction from the value of K is necessary since the intact coal seam is not completely saturated with the microbial media during bioconversion and only a fraction of the reservoir is actually bioconverted. However, the extent of bioconversion under in situ conditions is not known, thereby warranting the need for introduction of the variable $\varkappa$. The value of $\varkappa$ is arrived at using stress–strain inter-relationships, which will be detailed here. It should also be pointed out that a BCBM reservoir, while undergoing bioconversion, is not expected to be in production mode. The effect of the fourth term in Eq. (4), $\varkappa\widetilde{\epsilon_T}\delta_{ij}$, comes into effect only after the reservoir starts producing. The strains developed due to bioconversion will primarily affect the initial effective stress of the BCBM reservoir when production starts. This effect is captured in the model derived.

Equation (4) is the governing equation for effective stress of a BCBM reservoir undergoing depletion, that is, production of bio-generated methane. It can be modified for any boundary condition existing in the reservoir. Connell et al. (2010) presented a concise paper based on similar governing equation, where the *pdk* model for different boundary conditions of triaxial stress and strain was developed. In this paper, we consider a BCBM reservoir producing under uniaxial strain, where the reservoir is allowed displacement only in the Z direction but not in the X and Y directions, a condition most commonly believed to exist in CBM reservoirs. The derivation follows the model presented by Shi and Durucan (2004), but can be similarly applied to any other stress or strain based models, and any governing boundary conditions.

The stress–strain components for the three normal stresses, as derived from Eq. (4), can be presented as:

$$\widetilde{\sigma}_{xx} = 2G\widetilde{\epsilon}_{xx} + \lambda\widetilde{\epsilon} + K\widetilde{\epsilon_S} + \varkappa\widetilde{\epsilon_T} \tag{5a}$$

$$\widetilde{\sigma}_{yy} = 2G\widetilde{\epsilon}_{yy} + \lambda\widetilde{\epsilon} + K\widetilde{\epsilon_S} + \varkappa\widetilde{\epsilon_T} \tag{5b}$$

$$\widetilde{\sigma}_{zz} = 2G\widetilde{\epsilon}_{zz} + \lambda\widetilde{\epsilon} + K\widetilde{\epsilon_S} + \varkappa\widetilde{\epsilon_T} \tag{5c}$$

The in situ condition during CBM production is known to be under uniaxial strain, where the vertical stress resulting from the weight of the overburden rock remains constant and the coal is free to compress in the vertical (Z) direction. However, since the horizontal extent of the reservoir is confined, there is no lateral movement, thus $\widetilde{\epsilon}_{xx} = \widetilde{\epsilon}_{yy} = 0$. Using this boundary conditions and following Shi and Durucan's (2004) derivation, the effective horizontal stress is expressed as:

$$\sigma - \sigma_0 = -\frac{\nu}{1-\nu}(p - p_0) + \frac{E}{3(1-\nu)}\epsilon_1\left(\frac{p}{p + P_\epsilon} - \frac{p_0}{p_0 + P_\epsilon}\right) + \varkappa\widetilde{\epsilon_T} \tag{6}$$

The subscript 0 refers to the initial values of the corresponding parameters. Equation (6) describes the variation in effective stress with continued reduction in reservoir pore-pressure of a producing BCBM reservoir. The parameter E is the Young's modulus and ν is the Poisson's ratio. In order to understand the variation of effective stress as a function of pore pressure, a function $f(p) = (\sigma_0 - \sigma)$ is defined which represents the reduction in the effective horizontal stress (Shi and Durucan 2004). Going forward, the function $f(p)$ will be referred to as the effective stress state. Formulation of $f(p)$ ensures that the cleat permeability varies positively with the effective stress state, expressed as (Shi and Durucan 2004):

$$\begin{aligned} f(p) = f_b(p) &= \left(\sigma_{b_0} - \sigma_b\right) \\ &= \frac{\nu}{1-\nu}\left(p - p_0\right) \\ &\quad \left[1 - \frac{E}{3\nu}\frac{\epsilon_1 P_\epsilon}{\left(p + P_\epsilon\right)\left(p_0 + P_\epsilon\right)}\right] \end{aligned} \tag{7}$$

Since one of the goals of BCBM technology is to recharge depleted CBM reservoirs and economically produce microbially generated methane, we use the subscript 'b' (for *before*) to denote the effective stress state during primary depletion. This is termed the primary depletion stage. Equation (7) is applicable to production from the CBM reservoir prior to bioconversion and does not have the $\varkappa\widetilde{\epsilon_T}$ term as there is no bioconversion involved. It is to be noted that the expression for $f_b(p)$ at $p = p_0$, expressed as $f_b(p_0)$ reduces to 0, since $(p_0 - p_0) = 0$. This boundary conditions will be used later to derive the expression for the modulus $\varkappa$. Similarly, post-treatment, subscript 'a' (for *after*) is used to describe what the stress state of the reservoir would be. Thus, the expression describing the stress state of the producing BCBM reservoir is given by Eq. (8). The post-treatment analysis is however done in comparison to the initial stress state of the reservoir before bioconversion. It is also important to mention that we assume that bioconversion will recharge the reservoir until it reaches the same initial pore-pressure that existed pre-bioconversion. Thus, $p_0 = p_{b_0} = p_{b_0}$.

$$\begin{aligned} f_a(p) &= \sigma_{b_0} - \sigma_a \\ &= \frac{\nu}{1-\nu}\left(p - p_0\right) \\ &\quad \left[1 - \frac{E}{3\nu}\frac{\epsilon_1 P_\epsilon}{\left(p + P_\epsilon\right)\left(p_0 + P_\epsilon\right)}\right] - \chi\widetilde{\epsilon_T} \end{aligned} \tag{8}$$

which can also be expressed as: $f_a(p) = f_b(p) - \varkappa\widetilde{\epsilon_T}$. Please note that the change in stress state during the life of a producing BCBM reservoir is evaluated in comparison to the initial stress state pre-bioconversion, i.e., σ_{b_0} and not σ_{a_0}. It is to be noted that the expression for $f_a(p)$ at $p = p_0$, expressed as $f_a(p_0)$ reduces to $-\varkappa\widetilde{\epsilon_T}$, since $(p_0 - p_0) = 0$. This boundary condition will also be used later to derive the expression for the modulus $\varkappa$.

Assuming a bundle of matchstick geometry, most commonly used to model flow in coal (Seidle 2011), the *pdk* response of a coalbed methane reservoir to primary depletion is typically expressed as:

$$\frac{k_{\mathrm{b}}}{k_{\mathrm{b0}}} = e^{3c_{\mathrm{f}}f_{\mathrm{b}}(p)} \tag{9}$$

where, k_{b0} is the initial permeability of the (virgin) reservoir, c_{f} is the cleat compressibility, and k_{b} is the reservoir permeability undergoing depletion. It is to be noted that the expression for Eq. (9), at initial condition, i.e., $k_{\mathrm{b0}}/k_{\mathrm{b0}}$ reduces to a value of 1, as the exponent to the exponential equates to 0. This boundary condition will be used to help derive an expression for the modulus $\varkappa$. Bioconversion induces fracture and matrix strains during treatment, which is expected to significantly affect the initial permeability of a BCBM reservoir compared to an untreated (virgin) CBM reservoir. The *pdk* response of a BCBM reservoir is now expressed using Eq. (10), where k_{a} is the permeability of the biogenic reservoir undergoing depletion.

$$\frac{k_{\mathrm{a}}}{k_{\mathrm{b0}}} = e^{3c_{\mathrm{f}}f_{\mathrm{a}}(p)} = e^{3c_{\mathrm{f}}f_{\mathrm{b}}(p)} \times e^{-3c_{\mathrm{f}}\varkappa\widetilde{\epsilon_T}} \tag{10}$$

It should be pointed out that Eq. (10) describes the *pdk* response of a coal reservoir post- bioconversion with respect to the initial permeability of the original reservoir (k_{b0}). Given that biogenic methane production from coal can exceed the sorptive (storage) capacity of the coal type (Pandey 2015; Pandey et al. 2016), it is expected that coal will be saturated with the produced biogenic methane given enough time for bioconversion. This will reverse the *pdk* effect of the depleted reservoir prior to commencement of bioconversion. Effectively, $\frac{k_{\mathrm{b}}}{k_{\mathrm{b0}}}$ and $\frac{k_{\mathrm{a}}}{k_{\mathrm{a0}}}$ of the reservoir would be the same unless there are changes in the sorptive and geomechanical behavior due to bioconversion. These changes have been studied and reported in the past (Pandey and Harpalani 2019b). However, given the importance of sorptive effects on the pressure-dependent permeability response of coal reservoirs, the combined effect of bioconversion induced strains and changes in sorptive behavior has also been analyzed in this work, detailed in Sect. 4.

Before we can effectively analyze the effective stress and *pdk,* as modeled by Eqs. (8) and (10) respectively, we need to derive an expression for $\varkappa$. The permeability-fracture porosity relationship, derived for the bundle of matchsticks geometry is cubic, where the variation in the reservoir permeability is directly proportional to the cube of its variation in cleat porosity (Cui and Bustin 2005; Palmer and Mansoori 1998; Seidle et al. 1992; Shi and Durucan 2005). The following derivation from Eq. (10) would then provide an expression for $\varkappa$.

$$\left(\frac{k_{\mathrm{b0}}}{k_{\mathrm{a0}}}\right) = e^{3c_{\mathrm{f}}\varkappa\widetilde{\epsilon_T}} / e^{3c_{\mathrm{f}}f_{\mathrm{b}}(p_0)} \tag{11}$$

The cubic permeability-fracture porosity relationship, where ϕ is fracture porosity, can be written as:

$$\left(\frac{k_{\mathrm{b0}}}{k_{\mathrm{a0}}}\right) = \left(\frac{\phi_{\mathrm{b}_0}}{\phi_{\mathrm{a}_0}}\right)^3 \tag{12}$$

Combining Eqs. (11) and (12) gives the following:

$$\left(\frac{\phi_{\mathrm{b}_0}}{\phi_{\mathrm{a}_0}}\right) = e^{c_{\mathrm{f}}\varkappa\widetilde{\epsilon_T}} \tag{13}$$

and,

$$\varkappa\widetilde{\epsilon_T} = \frac{1}{c_{\mathrm{f}}}\ln\left(\frac{\phi_{\mathrm{b}_0}}{\phi_{\mathrm{a}_0}}\right) \tag{14}$$

Images obtained pre- and post- bioconversion enable estimating k_{b0} and k_{a0} along with values for ϕ_{b_0} and ϕ_{a_0}. Section 3.1 provides a detailed overview of how images obtained before and after bioconversion were processed and analyzed to obtain the required data.

Equation (4), describing the stress state for a BCBM reservoir, can now be re-written as:

$$\widetilde{\sigma}_{ij} = 2G\widetilde{\epsilon}_{ij} + \lambda\widetilde{\epsilon}\delta_{ij} + K\widetilde{\epsilon}_{\mathrm{S}}\delta_{ij} + \frac{1}{c_{\mathrm{f}}}\ln\left(\frac{\phi_{\mathrm{b}_0}}{\phi_{\mathrm{a}_0}}\right) \tag{15}$$

Given that the focus of the work presented here is on effective stress state and *pdk*, pore volume referred here is the cleat/fracture pore volume. The porosity is thereby given as follows, where $V_{\bar{\mathrm{p}}}$ is the fracture pore volume and $V_{\bar{\mathrm{b}}}$ is the bulk volume:

$$\phi = \frac{V_{\bar{\mathrm{p}}}}{V_{\bar{\mathrm{b}}}} \tag{16}$$

It can be shown from Eq. (16) that (Connell et al. 2010; Cui and Bustin 2005):

$$\frac{\mathrm{d}\phi}{\phi} = \mathrm{d}\epsilon_T^{\bar{\mathrm{b}}} - \mathrm{d}\epsilon_T^{\bar{\mathrm{p}}} \tag{17}$$

where,$\epsilon_T^{\bar{\mathrm{b}}}$ is the bulk strain and $\epsilon_T^{\bar{\mathrm{p}}}$ is the fracture pore strain induced by bioconversion. The imaging results (discussed later) reveal that the matrix strain ($\epsilon_T^{\bar{\mathrm{m}}}$), along with the fracture pore strain, make up the bulk strain and this is negligible. The inter-relationship between the three strains along with the fracture porosity is given as follows (Liu and Harpalani 2014a):

$$\epsilon_T^{\bar{b}} = \phi\epsilon_T^{\bar{p}} + (1-\phi)\epsilon_T^{\bar{m}} \tag{18}$$

Integrating Eq. (17) gives the following:

$$\int_{\text{Pre}}^{\text{Post}} \frac{\mathrm{d}\phi}{\phi} = \int_{\text{Pre}}^{\text{Post}} \mathrm{d}\epsilon_T^{\bar{b}} - \int_{\text{Pre}}^{\text{Post}} \mathrm{d}\epsilon_T^{\bar{p}} \tag{19}$$

$$\equiv \ln\left(\frac{\phi_{\text{Post}}}{\phi_{\text{Pre}}}\right) = \epsilon_T^{\bar{b}} - \epsilon_T^{\bar{p}} \tag{20}$$

We can now rewrite Eqs. (15), (8) and (10) as Eqs. (21), (22) and (23) a, b respectively which, for a BCBM reservoir, define the poromechanical governing equation, and the effective stress state and *pdk* response under uniaxial strain respectively:

$$\widetilde{\sigma}_{ij} = 2G\widetilde{\epsilon}_{ij} + \lambda\widetilde{\epsilon}\delta_{ij} + K\widetilde{\epsilon}_{\text{S}}\delta_{ij} + \frac{1}{c_{\text{f}}}(\epsilon_T^{\bar{b}} - \epsilon_T^{\bar{p}}) \tag{21}$$

$$\begin{aligned} f_{\text{a}}(p) &= \sigma_{\text{b}_0} - \sigma_{\text{a}} \\ &= \frac{\nu}{1-\nu}(p-p_0)\left[1 - \frac{E}{3\nu}\frac{\epsilon_{\text{l}} P_\epsilon}{(p+P_\epsilon)(p_0+P_\epsilon)}\right] \\ &\quad - \frac{1}{c_{\text{f}}}\left(\epsilon_T^{\bar{b}} - \epsilon_T^{\bar{p}}\right) \end{aligned} \tag{22}$$

$$\frac{k_{\text{a}}}{k_{\text{b}0}} = e^{3c_{\text{f}}f_{\text{a}}(p)} = e^{3c_{\text{f}}\left[f_{\text{b}}(p) - \frac{1}{c_{\text{f}}}(\epsilon_T^{\bar{b}} - \epsilon_T^{\bar{p}})\right]} \tag{23a}$$

$$\frac{k_{\text{a}}}{k_{\text{b}0}} = e^{3c_{\text{f}}\left[\frac{\nu}{1-\nu}(p-p_0)\left\{1 - \frac{E}{3\nu}\frac{\epsilon_{\text{l}}P_\epsilon}{(p+P_\epsilon)(p_0+P_\epsilon)}\right\}\right] - 3(\epsilon_T^{\bar{b}} - \epsilon_T^{\bar{p}})} \tag{23b}$$

3 Strain quantification

Characterizing bioconversion induced strains requires quantification of fracture-pore and matrix strains. The two strains are estimated using two different approaches: image analysis for fracture strains, and continuous strain monitoring for matrix strains. In order to quantify the fracture strains resulting from bioconversion, we analyzed the images presented in a prior publication (Pandey and Harpalani 2018), a part of the same broader study. However, the imaging approach does not provide reliable estimates of matrix strains. In order to characterize this, matrix strain was recorded on a coal sample undergoing bioconversion. The experimental setup and results are presented in the following section, including analysis of the results. The measured strain was then used as a model input parameter to analyze a BCBM reservoir response.

3.1 Fracture pore strain

Pandey and Harpalani (2018) presented the changes in coal structure due to bioconversion, based on results obtained from scanning microscopy imaging. Images captured before and after bioconversion provided quantifiable details of the variation in the pore structure of coal. Work presented here is based on two sets of representative images reported by previously (Pandey and Harpalani 2018), where the samples showed decrease in fracture width post-bioconversion. Using the standard level adjustment and segmentation techniques, we quantified the cleat/fracture porosity of the samples using publicly available software called ImageJ. Decrease in fracture width is expected to lower Darcian flow through the sample, an observation that is consistent with reported experimental data (Pandey and Harpalani 2019a; Stephen et al. 2014). Although limited instances of increase in fracture width were also reported by Pandey and Harpalani (2018), it is not considered for detailed analysis given that there is no apparent experimental correlation of increase in permeability of the sample post-bioconversion. However, the methods presented here are universally applicable for any measured changes in pore strain, and this aspect is further discussed in the appendix section. Figure 2 presents the fractures in two samples 1 and 2, before and after bioconversion. The porosity of the two samples was calculated by analyzing the ratio of black pixels to the total pixels in an image, post segmentation of the fractures from the coal matrix. The processed images for samples 1 and 2 are presented in Fig. 3. Results from image processing, along with the calculated fracture porosity values are presented in Table 1. The values for $\epsilon_T^{\bar{p}}$ were then calculated from the data shown in Table 1 and used as input to evaluate its effect on the response of a BCBM reservoir. As seen from Figs. 2 and 3, bioconversion resulted in swelling of the coal matrix, thereby reducing the fracture porosity. With the matrix swelling into open fractures, the fracture connectivity is expected to reduce, thereby blocking the path allowing for gas flow/seepage within the coal, effectively reducing permeability.

3.2 Matrix strain

Swelling strain due to bioconversion was measured experimentally during the process of bioconversion, and the results obtained were used to quantify $\epsilon_T^{\bar{m}}$. This value of $\epsilon_T^{\bar{m}}$ along with $\epsilon_T^{\bar{p}}$ were used in Eq. (18) to quantify $\epsilon_T^{\bar{b}}$. The fracture pore strain measurements were conducted on two different samples, and matrix strain measurement was conducted on a third sample sourced from the same source of coal. Evaluation of $\epsilon_T^{\bar{b}}$ and the subsequent analysis of permeability behavior assumed that $\epsilon_T^{\bar{m}}$ is the same for samples imaged given that they were sourced from the same block of coal during

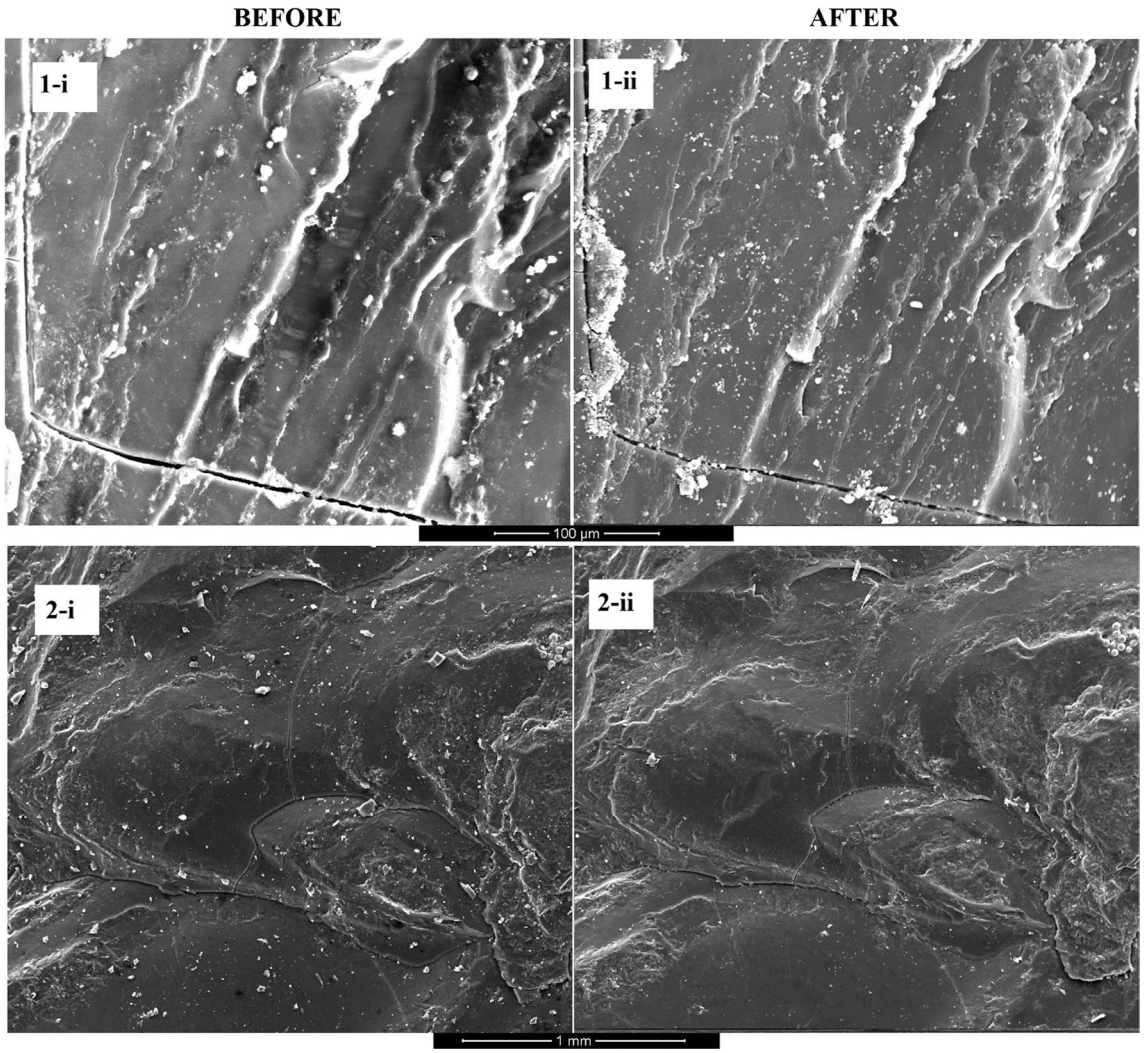

Fig. 2 SEM mages obtained from samples 1 and 2. (Pre (i)—and post (ii) -bioconversion)

sample preparation. Details of the experimental design and the results are discussed in this section.

3.2.1 Experimental design

The work reported here was a part of a broader study aimed at investigating the bioconversion potential of Illinois coals (Pandey 2015; Pandey and Harpalani 2018, 2019b, c; Saurabh and Harpalani 2018; Zhang et al. 2018a, b, 2015a, 2015a; Zhang and Liang 2017).

The experimental work was conducted on the same coal type, retrieved from Illinois 6 seam in Southern Illinois, weighing 36 g, using the same media engineered for bioconversion, used in the work cited above. The microbial media was engineered from produced water collected from a CBM wellhead and preserved under anaerobic conditions, as reported previously (Zhang et al. 2015a, b). Large coal blocks were sourced from an underground mine and preserved in a humid environment prior to sub-sampling for the experiment.

Experiments designed to capture the strain response of coal under different conditions have been reported extensively (Liu and Harpalani 2013, 2014a, b; Pandey and Harpalani 2019b). Sample preparation procedure for the experimental work was similar to that reported in Liu and Harpalani (2013). A smaller coal sample was retrieved from the larger block that was preserved under humid conditions. Three strain gages, attached orthogonally, captured the strain behavior in the X, Y and Z directions, with the Z direction being perpendicular to the bedding plane. The sample was then placed in a humidity and temperature environmental chamber to achieve moisture equilibrium. Following this, the sample was placed in a high-pressure vessel, which facilitated connection of the strain gages and pressure transducer to the data acquisition system designed to monitor pressure and sample strain response. This constituted the strain aspect

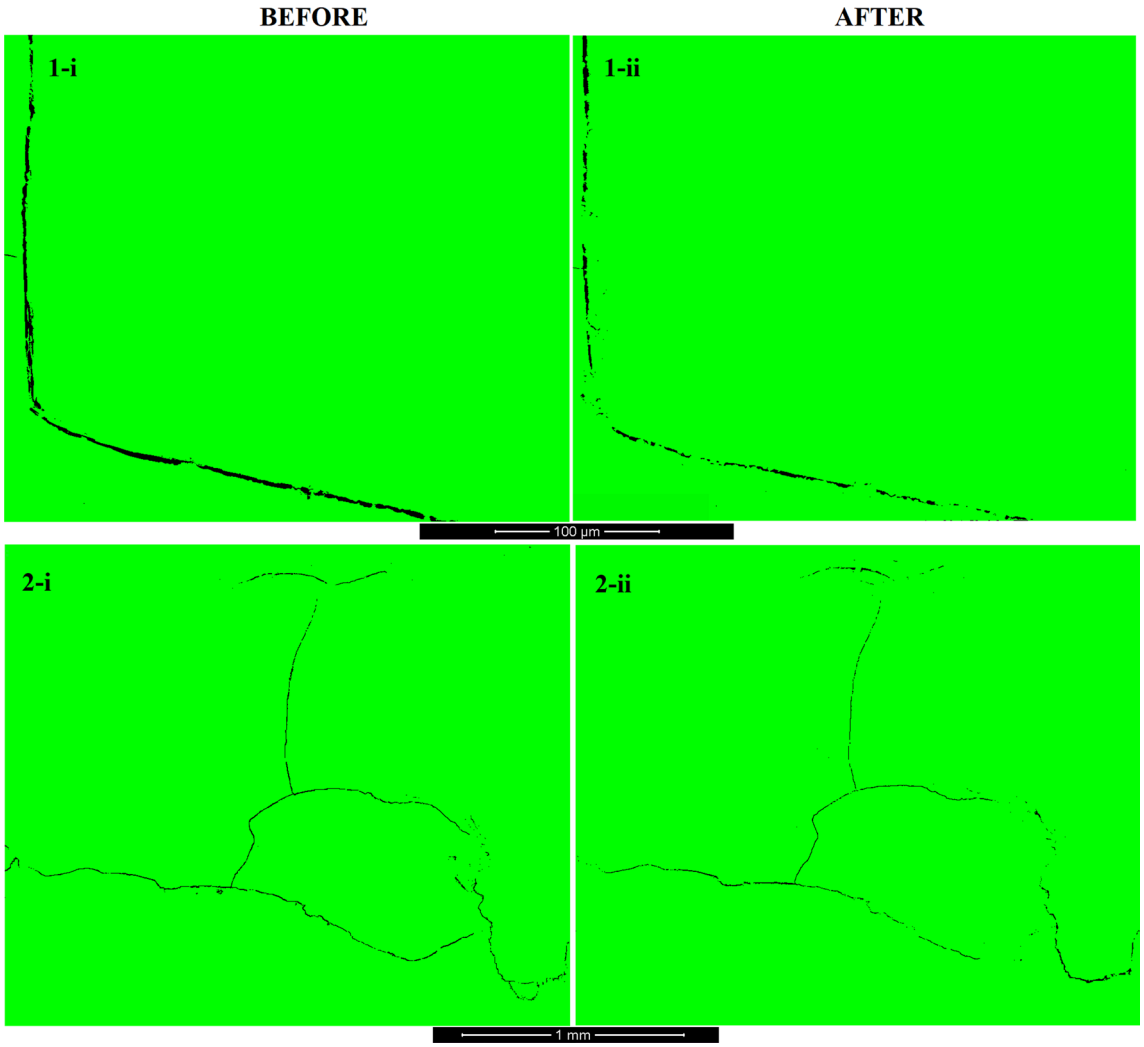

Fig. 3 Processed images from samples 1 and 2, where the fracture porosity decreased post treatment. (Pre (i)—and post (ii) -bioconversion)

Table 1 Image properties

Sample No.	Condition (Image)	Total pixels	Black pixels	Fracture porosity (%)	Fracture pore strain $\epsilon_T^{\bar{p}}$
1	Before (1-i)	908,010	9310	1.025	0.492
	After (1-ii)	901,404	4699	0.521	
2	Before (2-i)	890,618	4207	0.47	0.255
	After (2-ii)	889,974	3105	0.35	

of the experiment. The sample was submerged in ~ 400 ml of the nutritionally amended microbial solution. The headspace in the pressure vessel was huffed-and-puffed with helium, and the pore-pressure was increased to ~ 30 psi, to ensure the headspace was completely lacking in oxygen. The entire experimental setup was placed in a water bath, capable of maintaining a constant temperature of 32 °C. The sample and pressure container used is shown in Fig. 4.

Pore pressure was also monitored along with the strains. Intermittent gas sampling was not conducted since the experiment was designed to replicate the practical application, where production would commence only after coal was bioconverted over a specific duration, 30 days in our case,

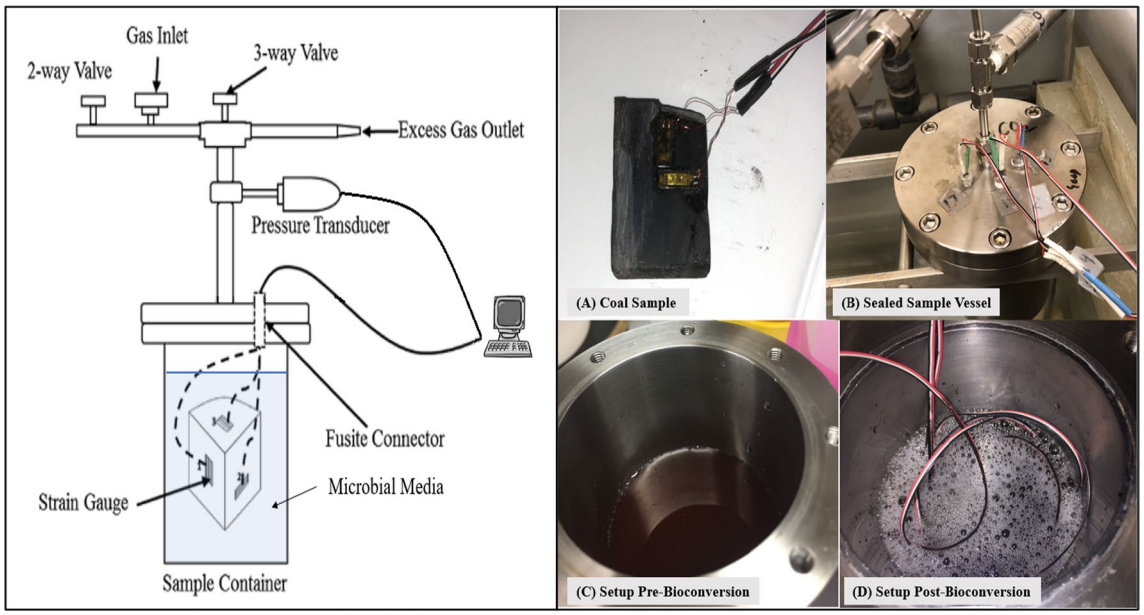

Fig. 4 Schematic of the experimental setup is shown on the left. The setup is maintained at a constant temperature water bath. **a** Coal sample used for bioconversion, with strain gages attached orthogonally **b** Sealed sample vessel **c** Pressure reactor before bioconversion **d** Pressure reactor after bioconversion

after which the headspace was depressurized. Post-treatment period, the gas content was measured using a gas chromatograph. The strain response was also monitored post depletion in order to obtain the irreversible residual swelling induced due to bioconversion.

3.2.2 Experimental results

The coal tested produced equivalent of 472 scft of methane over the thirty-day treatment period. Figure 4 shows the open container before (Fig. 4c) and after (Fig. 4d) bioconversion. Methane production over the treatment period resulted in the frothy media, as seen in the image. The goal of this setup was to capture the strain behavior of the sample. Strains in the X, Y and Z directions, represented as $\widetilde{\epsilon}_{xx}$, $\widetilde{\epsilon}_{yy}$ and $\widetilde{\epsilon}_{zz}$, were measured continuously, every 60 s over the treatment period. The total swelling (bulk) strain ($\widetilde{\epsilon}_V$), which is the sum of strains in the three orthogonal directions is represented by Eq. (24):

$$\tilde{\epsilon}_V = \epsilon_T^{\overline{m}} = \left(\tilde{\epsilon}_{xx} + \tilde{\epsilon}_{yy} + \tilde{\epsilon}_{zz}\right) \tag{24}$$

The strain response resulting from bioconversion is presented in Fig. 5. During the initial treatment period, the sample shrank with bioconversion. The maximum shrinkage was measured to be -0.0007 at the 5-day mark. The sample then started to swell, and the volumetric strain attained a positive value just before the 10th day of treatment. Swelling continued for the following thirteen days, and the maximum measured volumetric strain was ~ 0.0057. Post 23-day mark, the volumetric strain in the sample levelled off. The final volumetric strain observed at the end of 30 days was ~ 0.005. The headspace pressure was then relieved, and the system was brought to atmospheric pressure. The strains were continually monitored during and post-depletion until the strains normalized. The final residual matrix strain ($\epsilon_T^{\overline{m}}$) measured in the sample was ~ 0.0038.

The gas pressure in the headspace of the setup was monitored continuously over the duration of treatment. The sample was initially subjected to a pore pressure of ~ 30 psi. The variation of the headspace pressure is shown in Fig. 5. The pore pressure remained constant over the first twelve days. Past this, there was an exponential increase in the monitored headspace pressure, reaching ~ 63 psi in nine days. The pore pressure then levelled off and remained constant for the remaining treatment period.

The variation in headspace pressure correlates perfectly ($R^2 > 0.96$) with the observed volumetric strain induced in the sample, as shown in Fig. 5. The coal sample exhibited shrinkage over the initial five days of treatment. Such behavior is likely in response to the applied pore pressure. Following the five-day mark, the sample swelled continuously for 20 days. Such behavior can be explained by adsorption of produced methane in the coal matrix (along with bioconversion induced swelling) resulting in matrix swelling since methane in sorbed state does not contribute to measurable pressure. The increase in headspace pore pressure was observed only after twelve days. As methane

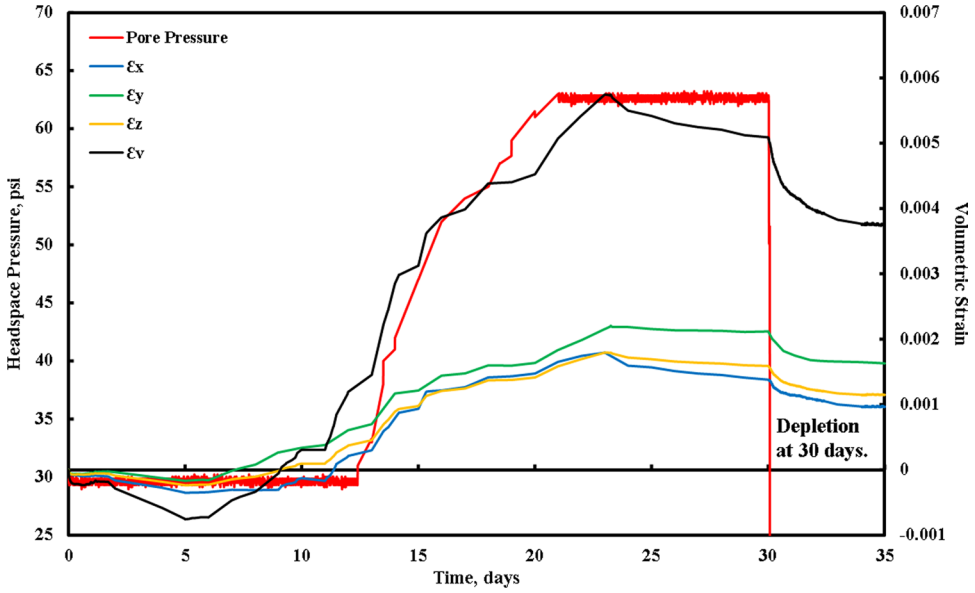

Fig. 5 Pore pressure variation and induced matrix strain with continued bioconversion

sorption continued over time, the rate and volume of sorption decreased, resulting in the produced methane bubbling out of the media and increasing the headspace pressure.

4 Insights into the reservoir behavior

The measured fracture-pore and matrix strains developed in coal due to bioconversion (at the laboratory scale) were used to evaluate their impact on the response of a BCBM reservoir. These were incorporated in the model presented in Sect. 2 in order to evaluate the effective stress state and pressure dependent permeability response of a BCBM reservoir with depletion. The model requires additional parameters, Langmuir's strain constants, Poisson's ratio, Young's modulus and cleat compressibility. Values of these input parameters were taken from previously published work for samples from the same block of coal ($\epsilon_l = 0.0145$, $P_\epsilon = 1200$ psi, $\nu = 0.4$, $E = 307{,}000$ psi, $c_f = 0.003$ psi^{-1}) (Mitra 2010; Pandey and Harpalani 2019b). However as previously reported, the process of bioconversion suppresses the sorptive strain response (Pandey and Harpalani 2019b). The sorption-induced strains arise from the response of the organic fraction (maceral) of the coal fabric to sorptive gases since microbial treatment converts this to biogenic methane. Loss of organic component results in suppression of the sorptive strain response (Meng et al. 2018) of coal and its impact on the reservoir response is important in the overall evaluation of the BCBM reservoir behavior. Hence, in Sects. 4.1.1 (effective stress state) and 4.1.2 (*pdk* response), the effects of bioconversion induced strains on reservoir parameters are first discussed in isolation, assuming no change in the other parameters. The effect of variation in sorptive-strain response is then included along with the effects of bioconversion induced strains. The relevant parameters reflecting pre- and post- bioconversion are presented in Table 2, where the subscripts 'b' and 'a' refer to the values 'before' and 'after' bioconversion. This necessitated modifying the expressions for effective stress state (*f(p)*) (Eqs. (25), (26)) and *pdk* response (Eqs. (27), (28)) of the reservoirs pre- and post- bioconversion as:

$$f_b(p) = \frac{\nu}{1-\nu}(p-p_0)\left[1 - \frac{E}{3\nu}\frac{\epsilon_{lb}P_{\epsilon b}}{(p+P_{\epsilon b})(p_0+P_{\epsilon b})}\right] \quad (25)$$

$$f_a(p) = \frac{\nu}{1-\nu}(p-p_0)\left[1 - \frac{E}{3\nu}\frac{\epsilon_{la}P_{\epsilon a}}{(p+P_{\epsilon a})(p_0+P_{\epsilon a})}\right] - \frac{1}{c_f}\left(\bar{\epsilon}_T^{\bar{p}} - \bar{\epsilon}_T^{\bar{b}}\right) \quad (26)$$

$$\frac{k_b}{k_{b0}} = e^{3c_f\left[\frac{\nu}{1-\nu}(p-p_0)\left\{1-\frac{E}{3\nu}\frac{\epsilon_{lb}P_{\epsilon b}}{(p+P_{\epsilon b})(p_0+P_{\epsilon b})}\right\}\right]} \quad (27)$$

$$\frac{k_a}{k_{b0}} = e^{3c_f\left[\frac{\nu}{1-\nu}(p-p_0)\left\{1-\frac{E}{3\nu}\frac{\epsilon_{la}P_{\epsilon a}}{(p+P_{\epsilon a})(p_0+P_{\epsilon a})}\right\}\right]-3(\epsilon_T^{\bar{b}}-\epsilon_T^{\bar{p}})} \quad (28)$$

Table 2 Sorption-induced strain behavior for samples pre- and post-bioconversion

Sample	ϵ_l	P_ϵ (psi)
Before	$\epsilon_{lb} = 0.0145$	$P_{\epsilon b} = 1200$
After	$\epsilon_{la} = 0.0055$	$P_{\epsilon a} = 600$

4.1 Effective stress

In this section, we model the effective stress state response (to depletion) of the two samples before and after bioconversion. The results are then interpreted in order to understand the effect of bioconversion on the effective stress-state (*f(p)*). The microbial treatment introduces two distinct effects on coal, the bioconversion induced strains and suppression of the sorptive strain behavior. The individual impact of the two effects on the modeled stress state was considered. The effective stress state (*f(p)*) was initially modeled for during primary depletion using Eq. (7). Since all samples were sourced from the same block, the primary depletion trend was the same, which is represented by the blue plot in Figs. 6a and b. With reduction in pore pressure, the value of *f(p)* increases. An increase in the value of *f(p)* is better from a reservoir's flow perspective. Contrary to conventional natural gas reservoirs, due to the unique property of desorption induced matrix shrinkage in CBM reservoirs, the effective stress state often improves with continued depletion (reduction in pore pressure), making the reservoir more conducive to Darcian flow.

Hence, an increase/decrease in the value of *f(p)* is indicative of an improvement/deterioration of the effective stress state respectively. When considering only the effect of bio-strains, as modeled by Eq. (22), both samples (red plots in Fig. 6) show a significant deterioration in the stress state. This is proportional to the decrease in cleat/fracture porosity due to bioconversion, as reported in Table 1. This indicates that the effective stress state deteriorates, thereby hindering fluid flow in the reservoir.

We now consider the effect of bioconversion-induced-strain and the suppression of sorption induced strain due to bioconversion on the effective stress state. It is assumed that both samples had an equal decrease in sorptive-strain response post-treatment, as indicated in Table 2. The effective stress state for samples 1 and 2 deteriorated significantly, as presented by the black plots in Figs. 6a and b respectively. This is due to the dual-negative effect of reduced porosity and suppressed sorptive strain response post-bioconversion. Thus, the effective stress state represented by these two samples continued to be negative throughout depletion. This implies that the reservoirs represented by the samples post-bioconversion will never revert back to the initial stress state (*f(p)* at 500 psi) of the original CBM reservoir.

4.2 Permeability

Bioconversion induced strains

The pressure dependent permeability (*pdk*) response of a BCBM reservoir represented by the samples was modeled using Eq. (23). Similar to the analysis for effective stress, changes in permeability during primary depletion were carried out using Eq. (9). Figures 7a and b present the *pdk* response of the two samples. In both figures, the blue plots show the *pdk* response during primary depletion. As seen in Sect. 4.1.1, since the effective stress state improved with depletion, given the combined effects of depletion induced increase in effective stress and matrix shrinkage, the permeability increased continuously with primary depletion. The permeability after primary depletion was ~ 34 times k_{b0}. Given that the modeled loss of effective stress state for reservoirs represented by samples 1 and 2, as seen in Fig. 7a and b, the modeled permeability values for the two cases also decreased. The initial permeability (k_{a0}) for bioconverted samples 1 and 2 was ~ 0.23 and 0.46 times k_{b0}, corresponding to the fracture-pore strains for the two samples, as seen

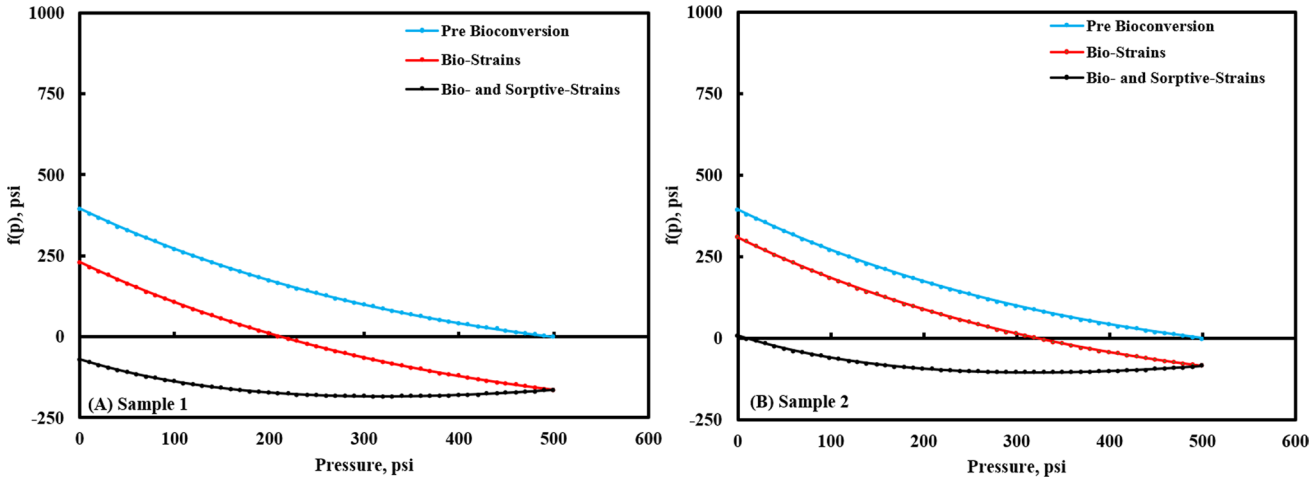

Fig. 6 Variation in effective stress state of reservoirs represented by **a** sample 1 and **b** sample 2 accounting for bioconversion induced and suppressed sorptive strains

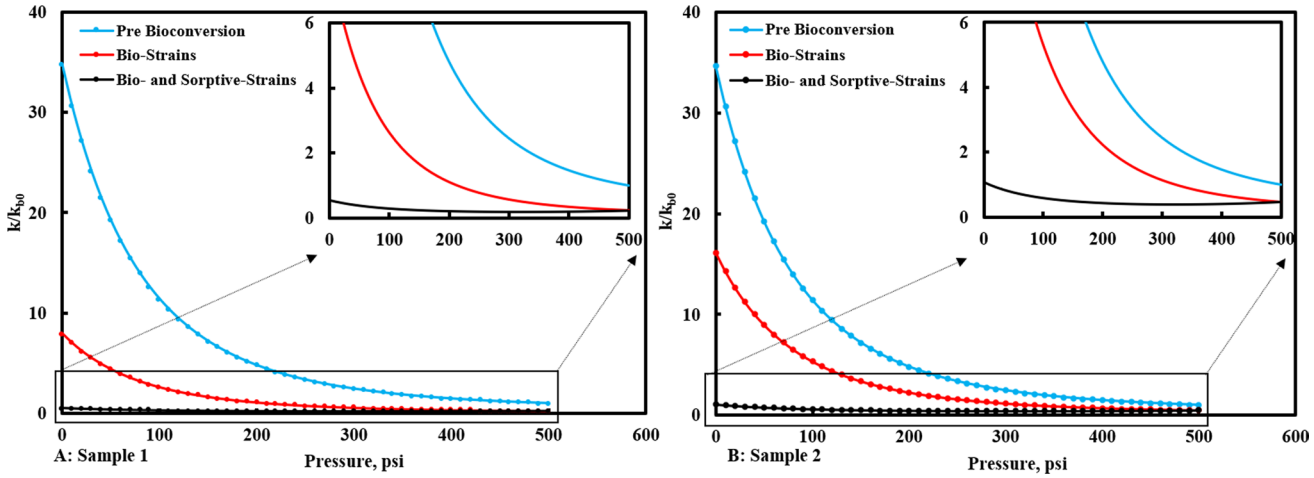

Fig. 7 Variation in permeability of reservoirs represented by **a** sample 1 and **b** sample 2 accounting for bioconversion induced and suppressed sorptive strains

in Table 1. The decrease in porosity post-bioconversion also suppressed the permeability increase observed during the primary depletion stage. The modeled permeability of the BCBM reservoir at complete depletion was ~ 8 and 16 times k_{b0} for samples 1 and 2 respectively.

Bioconversion induced and suppressed sorptive strains

The *pdk* response of the BCBM reservoirs was modeled using Eq. (28), considering the combined effect of bioconversion induced strains and suppression of sorptive strains. The *pdk* response during primary depletion (blue plot) however remained the same. Since (de)sorption induced (shrinkage) strains widens the cleat apertures, resulting in increased flow rates, the suppression of this behavior would hinder the flow rates. The *pdk* response, considering the combined effects of bioconversion induced strain and suppression of sorptive strains is shown in the black plots of Figs. 7a and b for samples 1 and 2 respectively. The *pdk* response, considering the combined effects, was almost flat with a near constant value of 0.2 and 0.5 times k_{b0} for samples 1 and 2 respectively.

5 Experimental correlation

The permeability results modeled above do not provide the measured flow rates through the coal sample, rather an interpretation of the expected reservoir behavior. Estimating the actual effect of bioconversion on the flow-coupled geomechanical response of the reservoir requires experimental validation. Limited studies have been reported that measured the variation in coal permeability due to bioconversion under stressed conditions. One reported study, conducted at the University of Alberta (Stephen et al. 2014) on a pack of crushed coal fines (sized at − 70 + 100 mesh), reported results for bioconversion for a period of 90 days. The permeability of the coal pack (Alberta 1) was estimated at different times during flooding with the microbial media. The Alberta 1 results, shown in Fig. 8, indicated a continuous decrease in permeability with continued bioconversion. The final permeability (k_{a0} = 5.2 mD) post-bioconversion was ~ 60% lower compared to pre-treatment permeability (k_{b0} = 13.3 mD).

Since the sample was crushed and packed, the physical characteristics of the coal structure was lost. To overcome this, two intact whole coal cores from the Illinois basin were bioconverted for a period of 60 days (Pandey and Harpalani 2019c). The permeability of the samples was estimated pre- and post- bioconversion. The results, presented in Table 2, revealed a decrease in the permeability of coal cores, similar to the tests conducted at University of Alberta. The final permeability (k_{a0}) of the two samples tested, SIU 1 and SIU

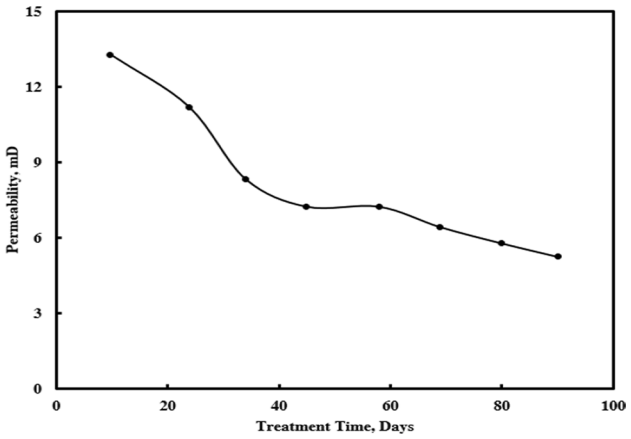

Fig. 8 Permeability variation of a coal-fine pack over 90 days of bioconversion. (adapted from Stephen et al. 2014)

Table 3 Permeability (mD) of two samples pre- and post- 60 days of replicated in situ bioconversion

Condition	Sample SIU 1	Sample SIU 2
Before	1.09	0.32
After	0.33	0.18

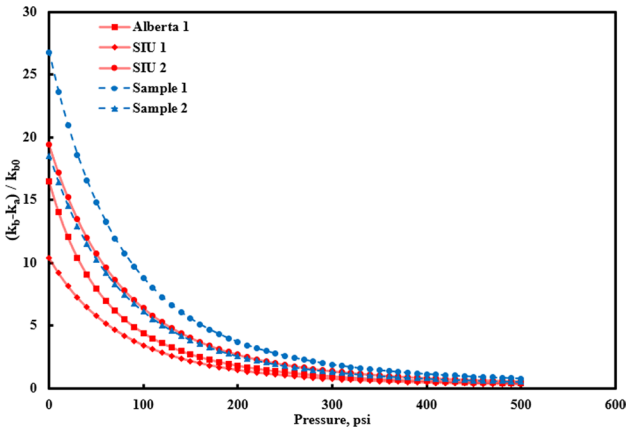

Fig. 9 Modeled decrease in pdk behavior due to bioconversion

2, was 0.30 and 0.56 times its initial permeability (k_{b0}) prior to bioconversion.

The permeability values obtained from the three (Alberta 1, SIU 1, SIU 2) samples were then used along with previously reported data (Bustin and Clarkson 1998; Clarkson and Bustin 1996; Pandey and Harpalani 2019b; Sabir and Chalaturnyk 2009) of E,ν, ϵ_l and P_ϵ for the two coal-types (Alberta and Illinois) to obtain the *pdk* behavior of the coal reservoirs pre-bioconversion ($\frac{k_b}{k_{b0}}$) and post-bioconversion ($\frac{k_a}{k_{b0}}$). It was assumed that the parameters, cleat compressibility and sorption induced shrinkage, remained unchanged during bioconversion. Additionally, characterizing the $\frac{k_a}{k_{b0}}$ behavior requires estimation of bioconversion induced strains. However, the permeability results obtained for Alberta-1, SIU-1 and SIU-2 samples do not directly provide values for bioconversion induced strains. Simple mathematical operations on Eqs. (9), (10), (12) and (14) made it possible to estimate the bioconversion induced strains from the reported permeability data in Table 3.

Since the experimental results indicate a reduction in coal permeability post-bioconversion, the $\frac{k_b}{k_{b0}}$ and $\frac{k_a}{k_{b0}}$ are not presented. Instead, we report the decrease in the *pdk* ratio post-bioconversion. In doing so, we use the following expression (decrease in *pdk* ratio): $\frac{k_b - k_a}{k_{a_0}}$, which is plotted against pore pressure. Figure 9 presents the 'decrease in *pdk* ratio' of the reservoir post-bioconversion for the experimental samples (Alberta 1, SIU 1 and SIU 2) and also for Samples 1 and 2 from the imaging experiment.

Figure 9 shows that the permeability of the BCBM reservoir post-bioconversion (represented by Alberta-1, SIU-1, SIU-2, Samples 1 and 2) will assume a lower value, compared to permeability of the original CBM reservoir pretreatment, thereby a positive decrease. This effect is magnified exponentially as the reservoir is depleted further, with the lowest value at the start of depletion (pore pressure of p_0 = 500 psi). The unique characteristic of CBM reservoirs is that, as the pore pressure decreases with depletion, the reservoir permeability increases due to the dominating effect of desorption-induced shrinkage. Suppression of the modeled permeability rebound of BCBM reservoirs would serve to hinder the production rates, especially in reservoirs where low-permeability is already a bottleneck to production. Figure 9 further shows that the decrease in initial permeability (k_{b0}–k_{a0}) and the modeled 'decrease in *pdk* ratio', predicted by imaging sample 2, were similar to the experimental results obtained for sample SIU 1. In comparison, imaged sample 1 over-predicts the decrease when compared to the three sets of experimental results. The absence of confining stresses and pore pressures during imaging and treating the samples can be attributed to the over-estimation. This aspect needs to be investigated further and is beyond the scope of the work presented here.

6 Modeling of expected field scale behavior

The work presented allows predicting the reservoir response of a BCBM operation. A BCBM operation is expected to have three stages where, in the first stage, the original CBM reservoir is depleted of its methane content, following which, the reservoir is recharged using microbial methods (stage 2). In the third stage, the biogenic methane produced is extracted. Since experimental investigations and imaging insights primarily revealed decrease in the fracture porosity of coal post-bioconversion, we consider the case where a reservoir is represented by sample 1. However, for the sake of completion, results from modeling efforts, where the sample exhibited increase in fracture porosity is discussed in the Appendix section. Figure 10 presents the modeling (permeability response) results for samples 1. The *pdk* response (k/k_{b0}) is plotted using logarithmic scale on Y axis as a function of pore pressure. During the first stage permeability of the original CBM reservoir increased with depletion. At the end of stage 1, reservoir permeability was ~ 34 times the initial permeability (k_{b0}). This is followed by the recharge stage. During this period, the produced biogenic methane is stored in the reservoir, resulting in swelling of the coal

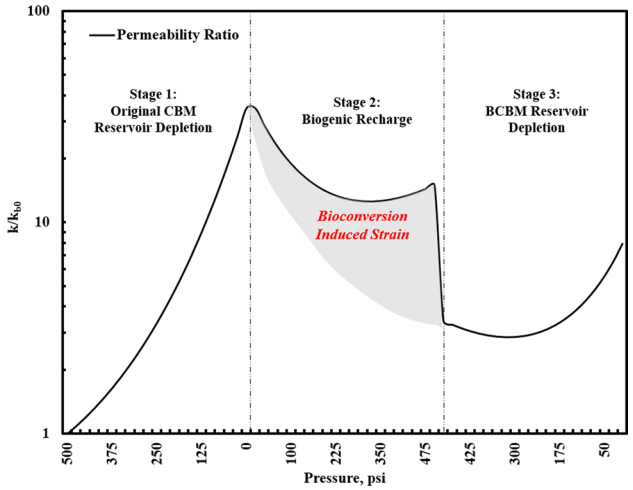

Fig. 10 Modeled *pdk* response of a BCBM reservoir represented by sample 1

matrix and a permeability decrease. However, since bioconversion suppresses the sorption-induced-strain behavior of coal, the permeability of the treated reservoir would be higher than k_{b0}, which in our case was ~ 15 times k_{b0}. In the third stage, when the biogenic methane is extracted, bioconversion induced strains plays a vital role in determining the reservoir's permeability response. For sample 1, as seen in Fig. 10, the decrease in porosity will result in a drop in the permeability. Modeling the results indicate that, at the start of stage 3, the reservoir permeability is ~ 3.3 times k_{b0}. It needs to be pointed out that bioconversion induced strains are developed continuously during the period of bioconversion (stage 2). Imaging approach only captures the 'before and after snapshot' and that for free standing sample. Thus, the reservoir permeability most likely deteriorated throughout the second stage, as indicated by the gray-highlighted region in Fig. 10. However, the exact path resulting in this deterioration is not known and requires measurement of porosity throughout the treatment duration, which is beyond the scope of the work presented here. The negative effect of lower cleat/fracture porosity post-bioconversion and suppressed sorptive strains, as seen in sample 1, festers itself throughout the third stage where, at complete depletion, the reservoir permeability was ~ 8 times k_{b0}.

The modeling results indicate that the low-permeability coal, containing narrow fractures, do not provide an ideal site for in situ BCBM production. Thus, coal deposits, such as in the Illinois Basin, do not provide suitable sites for in situ BCBM production. Operators are encouraged to target coal seams with higher initial permeability, such as in the Powder River or San Juan basins. This will ensure that, even with deterioration of effective stress state and reduced *pdk* response, the flowrates will be sufficiently high to justify economic biogenic methane production rates. This is especially true for depleted CBM reservoirs in such formations as, during depletion of a virgin CBM reservoir, there is significant loss of stress state, and the coal is even suspected to rubblize during depletion, thus increasing its fracture porosity/permeability significantly. Application of bioconversion to such deposits can increase flow rates exponentially, thus providing a site selection criterion for potential BCBM reservoirs.

7 Summary and conclusions

Work presented in this paper quantifies the matrix, pore and bulk strains developed in coal due to bioconversion. Fracture-pore strain data was obtained from imaging experiments. For the first time in reported literature, experiments developed to monitor matrix bio-strain during bioconversion were carried out and the resulting strain data presented. Additionally, in order to understand the effect of bioconversion on the geomechanics-coupled-flow response of a BCBM reservoir, a poromechanical model was developed. The developed model was then used to understand the effect of bioconversion on the effective stress state and pressure-dependent-permeability response of a BCBM reservoir during depletion.

Estimation of pressure dependent permeability response due to bioconversion, as estimated using imaging approaches was validated by experimental measurements of flow. The results revealed a significant loss in reservoir permeability post bioconversion. The loss in reservoir permeability will be a bottleneck to successful BCBM production from low permeability coals, like the Illinois basin. This aspect was further highlighted in the field-scale modeling results, where bioconversion-induced-strains along with suppressed sorptive strain response of coal severely restricted the permeability rebound in BCBM reservoirs, an aspect critical to successful BCBM operation.

However, the results also revealed that reservoirs with high initial permeability, prior to bioconversion will be better suited for in situ bioconversion. This will ensure that the reservoir will retain sufficient fracture porosity at the end of bioconversion to ensure economic BCBM production. Any prospective reservoir can now be analyzed based on the work presented here to assess suitability from a reservoir perspective, thus providing a preliminary *site selection criterion* for identifying potential coal deposits for BCBM production.

The heterogenous nature of coal, and the metabolic uncertainty associated with highly saturated in situ microbial environments presents a complex scientific problem when trying to understand BCBM reservoirs. In doing so, the work presented here captures *some* unique behaviors of coal samples when subjected to microbial conversion. Nevertheless, attaining a thorough comprehension of the procedure will

necessitate an in-depth examination, extending beyond the confines of the following:

(1) Understanding the effect of the organic (ex. macerals) and inorganic fractions (ex. metals and non-metals) in coal to the potential of bioconversion, and its subsequent effect on bioconversion induced swelling.
(2) Developing experiments in a highly controlled in situ environment, where microbial contamination during sampling, aerobic degradation of coal and produced water are minimized to provide the best representation of in situ environments. Additionally, conducting controlled bioconversion of coal under replicated in situ stress is also required to understand the expected reservoir-scale response of BCBM reservoirs.
(3) The effect of bioconversion on flow-coupled-geomechanical properties of coal, such as fracture compressibility, modulus of elasticity, strength, etc. need to be understood in more detail. In doing such experiments, given the destructive nature of the tests and the heterogenous nature of coal, samples should be selected based on a unified stress–strain pretest (under elastic deformation) approach to ensure selection of samples with similar mechanical characteristics.

Appendix

The appendix section highlights the effect of increase in cleat porosity, on the effective stress state and the pressure dependent permeability response of the reservoir when subject to bioconversion and depletion. Images reported in previously reported work (Pandey and Harpalani 2018), which showed an increase in cleat/fracture porosity post bioconversion have been used for the analysis in this section.

Figure 11 presents the SEM image of the sample A1, pre- and post-bioconversion. Figure 12 presents the processed image used to obtain pore-strain data. Table 4 computes the fracture-pore strain, where in this instance a $\epsilon_T^{\overline{p}}$ of − 1.619 is reported. The negative fracture-pore strain value is indicative of the increase in total fracture-porosity post-bioconversion. This is clearly evident in the images as the horizontal fracture shows an increase in fracture aperture after bioconversion. Using the approach presented in the work reported here, the effect of increased fracture porosity on the reservoir is quantified from an effective stress and pressure dependent permeability perspective. The matrix strain value, $\epsilon_T^{\overline{m}}$ has been assumed to be 0.0038, as obtained from the experiments reported in Sect. 3.4.2.

In Fig. 13, the baseline blue plot presents how the effective stress state (*f(p)*) evolves with continued depletion for a CBM reservoir subject to initial depletion, prior to bioconversion. Since microbial treatment results in bioconversion induced strains, which in this case resulted in an increase in cleat porosity, the modeled effective stress state improves significantly compared to the baseline, as seen in the red plot of Fig. 13. The value of *f(p)* at the reservoir pressure of 500 psi when considering the effect bioconversion induced strain is 540 times higher than the pre-bioconversion baseline value at 500 psi. As previously mentioned, an increase in the effective stress state is indicative of improved conditions promoting higher rates and volumes of fluid flow through the reservoir. At reservoir depletion (pore pressure ~ 0 psi), the modeled effective stress state for the reservoir when

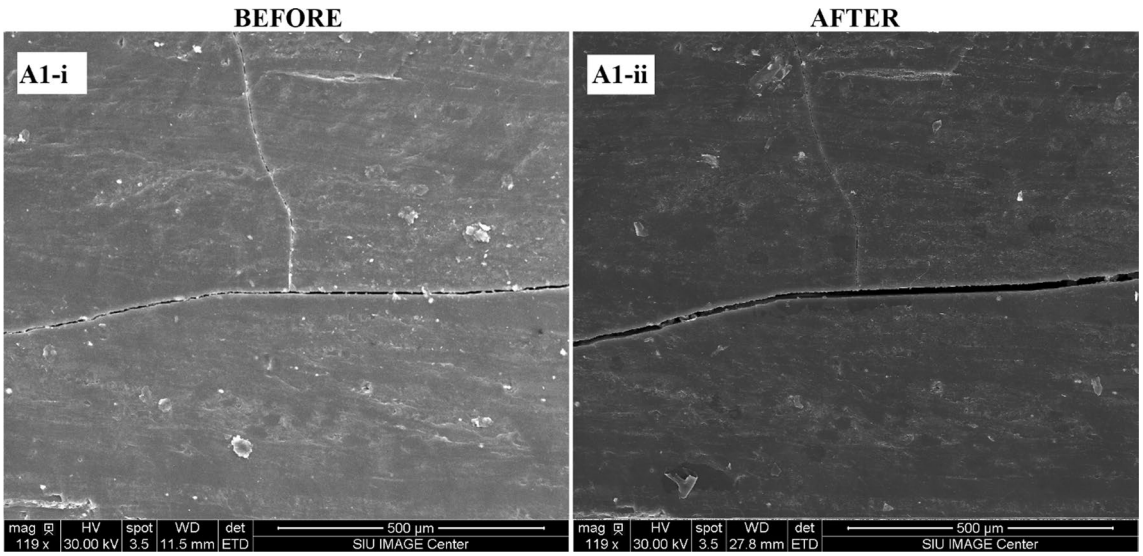

Fig. 11 SEM mages obtained from sample A1, pre (i)—and post (ii) -bioconversion

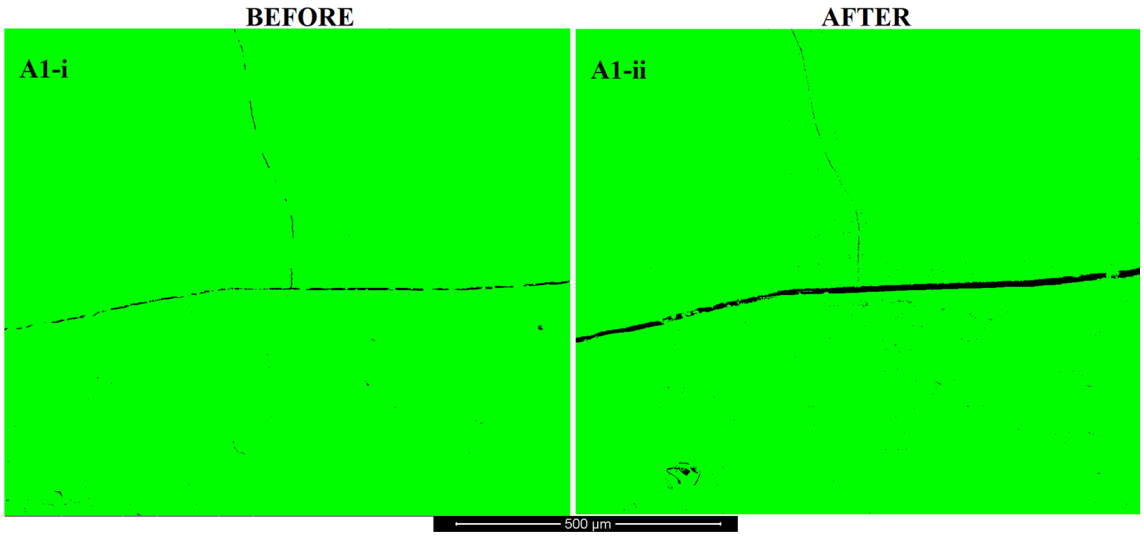

Fig. 12 Processed images from sample A1, where the fracture porosity increased post treatment. (pre (i)—and post (ii) -bioconversion)

Table 4 Image properties

Sample No.	Condition (Image)	Total Pixels	Black Pixels	Porosity (%)	Pore strain, $\epsilon_T^{\bar{p}}$
A1	Before (A1-i)	909,036	4083	0.449	− 1.619
	After (A1-ii)	901,263	10,602	1.176	

considering bioconversion induced strain is at 914 psi, which is 2.4 times the pre-bioconversion baseline value (of 380 psi).

Coal bioconversion also results in the suppression of the sorption induced strain response of the coal reservoir, which is detrimental from a reservoir perspective. The combined effect of bioconversion induced strain, and the suppression of sorptive strain is modeled and presented as the black plot in Fig. 13. It is evident that the suppression of the sorptive strain response limits the extent to which the reservoir's effective stress state improves. However, for sample A1, since the bioconversion induced strains improved the stress state significantly, the negative effect of suppressed sorptive strain was minimized. At reservoir depletion, considering the effect of both bioconversion induced strain and suppressed sorptive strain, the modeled value for *f(p)* was 618 psi, about 1.6 times the value at depletion for the pre-treated CBM reservoir.

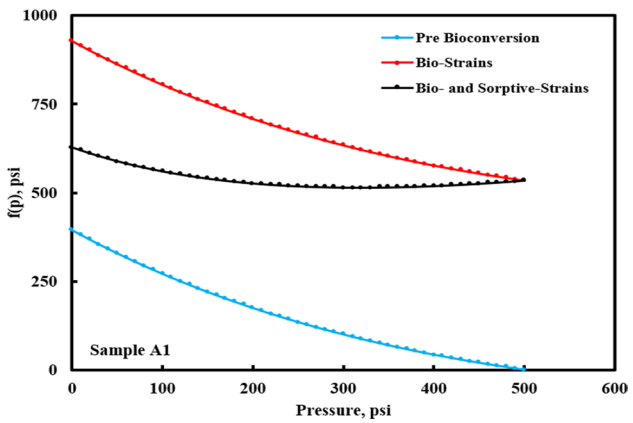

Fig. 13 Variation in effective stress state of samples A1 considering both bioconversion induced strain and suppressed sorptive strains

Figure 14 plots the pressure dependent permeability (*pdk*) of a BCBM reservoir represented by sample A1. Here, the blue plot shows the baseline *pdk* response during primary depletion, prior to bioconversion. As seen in Fig. 13, since the effective stress state improved with depletion, given the combined effects of depletion induced increase in effective stress and matrix shrinkage, the permeability also increased continuously with depletion. The permeability after primary depletion was ~ 34 times k_{b0}.

As sample A1 reported having an increase in fracture porosity, the bioconversion induced strain improved the reservoir permeability significantly compared to the baseline. This is evident in the red plot in Fig. 14, where permeability at depletion was ~ 4200 times k_{b0}. However, given the suppressed sorption-induced strain behavior of bioconverted coal, this exponential rise in reservoir permeability due to bioconversion induced strain was curtailed, where

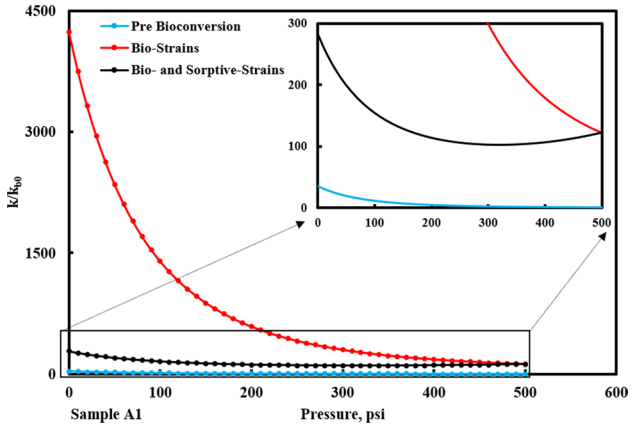

Fig. 14 Variation in permeability response of reservoir represented by sample A1, accounting for bioconversion induced and suppressed sorptive strains

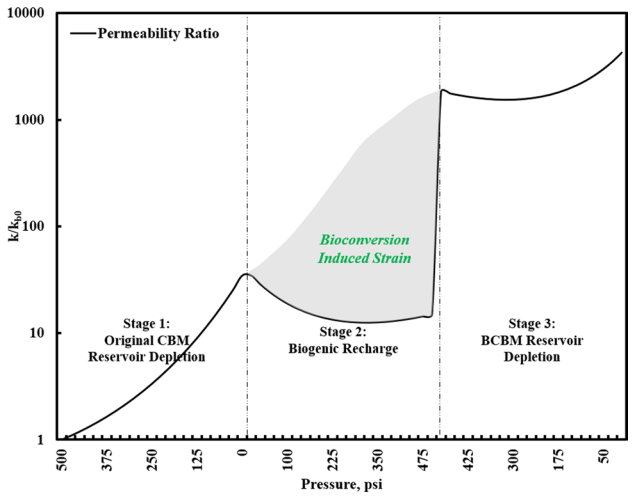

Fig. 15 Modeled *pdk* response of a BCBM reservoir represented by sample A1

the permeability at depletion was ~ 280 times k_{b0}, as seen in the black plot in Fig. 14. This observation highlights the sensitivity of a BCBM reservoir to pore strains.

Finally, Fig. 15 presents the modeling (permeability response) for sample A1. Similar to the result presented in Fig. 10, at the end of stage 1, reservoir permeability was ~ 34 times the initial permeability (k_{b0}). At the end of stage 2, the permeability of the reservoir was ~ 15 times k_{b0}. However, in the third stage, the bioconversion induced permeability played a vital role in determining the reservoir's permeability response. As seen in Fig. 15, at the start of stage 3, the reservoir permeability will be ~ 1800 times k_{b0}. It is pointed out again that the bioconversion induced strains are developed continuously throughout the period of bioconversion (stage 2), and the exact path of permeability increase is not known. The positive effect of higher fracture porosity post-bioconversion, as seen in sample A1 festers itself throughout the third stage, where at complete depletion, the reservoir permeability was ~ 4200 times k_{b0}. The modeling results thereby suggests that high-permeability reservoirs, containing wider fractures are better suited for BCBM production. This is especially true if the cleat/fracture porosity increases post-bioconversion, a possibility yet to be validated by in situ experimental results.

Acknowledgements The authors gratefully acknowledge support from the US Department of Energy, award number DE-FE0026161. The authors would also like to thank Dr. Yanna Liang and Ji Zhang for providing the optimized microbial media for bioconversion.

Author contribution RP - Theoretical development, experimental design, manuscript writing, results analysis. SH - Securing funding, manuscript editing, results analysis.

Open Access This article is licensed under a Creative Commons Attribution 4.0 International License, which permits use, sharing, adaptation, distribution and reproduction in any medium or format, as long as you give appropriate credit to the original author(s) and the source, provide a link to the Creative Commons licence, and indicate if changes were made. The images or other third party material in this article are included in the article's Creative Commons licence, unless indicated otherwise in a credit line to the material. If material is not included in the article's Creative Commons licence and your intended use is not permitted by statutory regulation or exceeds the permitted use, you will need to obtain permission directly from the copyright holder. To view a copy of this licence, visit http://creativecommons.org/licenses/by/4.0/.

References

Bear J, Corapcioglu MY (1981) A mathematical-model for consolidation in a thermoelastic aquifer due to hot water injection or pumping. Water Resour Res 17(3):723–736. https://doi.org/10.1029/WR017i003p00723

Bustin RM, Clarkson CR (1998) Geological controls on coalbed methane reservoir capacity and gas content. Int J Coal Geol 38(1–2):3–26. https://doi.org/10.1016/S0166-5162(98)00030-5

Clarkson CR, Bustin RM (1996) Variation in micropore capacity and size distribution with composition in bituminous coal of the Western Canadian Sedimentary Basin - Implications for coalbed methane potential. Fuel 75(13):1483–1498. https://doi.org/10.1016/0016-2361(96)00142-1

Connell LD, Lu M, Pan ZJ (2010) An analytical coal permeability model for tri-axial strain and stress conditions. Int J Coal Geol 84(2):103–114. https://doi.org/10.1016/j.coal.2010.08.011

Cui XJ, Bustin RM (2005) Volumetric strain associated with methane desorption and its impact on coalbed gas production from deep

coal seams. AAPG Bull 89(9):1181–1202. https://doi.org/10.1306/05110504114
Fallgren PH, Jin S, Zeng CP, Ren ZY, Lu AH, Colberg PJS (2013) Comparison of coal rank for enhanced biogenic natural gas production. Int J Coal Geol 115:92–96. https://doi.org/10.1016/j.coal.2013.01.014
Gray I (1987) Reservoir engineering in coal seams: part 1 - The physical process of gas storage and movement in coal seams. Spe Reserv Eval Eng 2(01):28–34. https://doi.org/10.2118/12514-PA
Harpalani S, Chen G (1997) Influence of gas production induced volumetric strain on permeability of coal. Geotech Geol Eng 15:303–325
Li D, Bao Y, Wang YY, An C, Chang JN (2023) Multiple-experimental investigation on the physicochemical structures alternation during coal biogasification. Fuel 339:127433. https://doi.org/10.1016/j.fuel.2023.127433
Liu SM, Harpalani S (2013) A new theoretical approach to model sorption-induced coal shrinkage or swelling. AAPG Bull 97(7):1033–1049. https://doi.org/10.1306/12181212061
Liu SM, Harpalani S (2014a) Compressibility of sorptive porous media: Part 1. Background and theory. AAPG Bull 98(9):1761–1772. https://doi.org/10.1306/03241413133
Liu SM, Harpalani S (2014b) Compressibility of sorptive porous media: Part 2. Experimental study on coal. Aapg Bull 98(9):1773–1788. https://doi.org/10.1306/03241413134
Meng Y, Liu SM, Li ZP (2018) Experimental study on sorption induced strain and permeability evolutions and their implications in the anthracite coalbed methane production. J Petrol Sci Eng 164:515–522. https://doi.org/10.1016/j.petrol.2018.01.014
Mitra A (2010) Laboratory investigation of coal permeability under replicated in situ stress regime Southern Illinois University Carbondale]. https://opensiuc.lib.siu.edu/dissertations/124/
Nowacki W (1970) Problems of thermoelasticity. Progress Aerosp Sci 10:1–63. https://doi.org/10.1016/0376-0421(70)90003-5
Opara A, Adams DJ, Free ML, McLennan J, Hamilton J (2012) Microbial production of methane and carbon dioxide from lignite, bituminous coal, and coal waste materials. Int J Coal Geol 96–97:1–8. https://doi.org/10.1016/j.coal.2012.02.010
Palmer I, Mansoori J (1998) How permeability depends on stress and pore pressure in coalbeds: A new model. SPE Reservoir Eval Eng 1(06):539–544. https://doi.org/10.2118/52607-PA
Pandey R, Harpalani S (2018) An imaging and fractal approach towards understanding reservoir scale changes in coal due to bioconversion. Fuel 230:282–297. https://doi.org/10.1016/j.fuel.2018.04.171
Pandey R, Harpalani S (2019b) Impact of bioconversion on matrix strain response of coal reservoirs: Part 1-Experimental insights. Fuel 239:1363–1375. https://doi.org/10.1016/j.fuel.2018.10.009
Pandey R, Harpalani S (2019c) *Modeling Fluid Flow Behavior in Microbially Recharged Coalbed Methane Reservoirs* Society for Mining, Metallurgy, and Exploration. Denver, USA
Pandey R, Harpalani S, Feng RM, Zhang J, Liang YN (2016) Changes in gas storage and transport properties of coal as a result of enhanced microbial methane generation. Fuel 179:114–123. https://doi.org/10.1016/j.fuel.2016.03.065
Pandey R, Harpalani S (2019a) *Evaluation of dynamic flow and production behavior of biogenic methane reservoirs* US Rock Mechanics/Geomechanics Symposium, New York
Pandey R (2015) Changes in properties of coal as a result of continued bioconversion Southern Illinois University Carbondale]. https://opensiuc.lib.siu.edu/theses/1745/
R., L. J. (1996) Model study of the influence of matrix shrinkage on absolute permeability of coal bed reservoirs. Geological Society 109:197–212. https://doi.org/10.1144/GSL.SP.1996.109.01.1
Sabir A, Chalaturnyk RJ (2009) Adsorption characteristics of coal in constant-pressure tests. Can Geotech J 46(10):1165–1176. https://doi.org/10.1139/T09-057
Saurabh S, Harpalani S (2018) Modeling of microbial methane generation from coal and assessment of its impact on flow behavior. Fuel 216:274–283. https://doi.org/10.1016/j.fuel.2017.12.015
Sawyer WK, Paul GW, Schraufnagel RA (1990) *Development And Application Of A 3-D Coalbed Simulator* Annual Technical Meeting. Calgary, Alberta
Scott AR (1999) Improving Coal Gas Recovery with Microbially Enhanced Coalbed Methane. Scientific, Environmental and Economic Evaluation, Coalbed Methane
Seidle JP, Jeansonne MW, Erickson DJ (1992) *Application of Matchstick Geometry To Stress Dependent Permeability in Coals* SPE Rocky Mountain Regional Meeting. Casper, Wyoming, USA
Seidle J (2011) *Fundamentals of coalbed methane reservoir engineering*. PennWell Corp. Publisher description http://www.loc.gov/catdir/enhancements/fy1214/2011019056-d.html
Shi JQ, Durucan S (2004) Drawdown induced changes in permeability of coalbeds: a new interpretation of the reservoir response to primary recovery. Transp Porous Media 56(1):1–16. https://doi.org/10.1023/B:TIPM.0000018398.19928.5a
Shi JQ, Durucan S (2005) A model for changes in coalbed permeability during primary and enhanced methane recovery. Spe Reserv Eval Eng 8(4):291–299. https://doi.org/10.2118/87230-Pa
Stephen A, Adebusuyi A, Baldygin A, Shuster J, Southam G, Budwill K, Foght J, Nobes DS, Mitra SK (2014) Bioconversion of coal: new insights from a core flooding study. RSC Adv 4(43):22779–22791. https://doi.org/10.1039/c4ra01628a
Strapoc D, Mastalerz M, Eble C, Schimmelmann A (2007) Characterization of the origin of coalbed gases in southeastern Illinois Basin by compound-specific carbon and hydrogen stable isotope ratios. Org Geochem 38(2):267–287. https://doi.org/10.1016/j.orggeochem.2006.09.005
Strapoc D, Picardal FW, Turich C, Schaperdoth I, Macalady JL, Lipp JS, Lin YS, Ertefai TF, Schubotz F, Hinrichs KU, Mastalerz M, Schimmelmann A (2008) Methane-producing microbial community in a coal bed of the Illinois basin (vol 74, pg 2424, 2008). Appl Environ Microbiol 74(12):3918–3918. https://doi.org/10.1128/Aem.00856-08
Table of contents only http://www.loc.gov/catdir/enhancements/fy1214/2011019056-t.html
Wawrik B, Mendivelso M, Parisi VA, Suflita JM, Davidova IA, Marks CR, Van Nostrand JD, Liang YT, Zhou JZ, Huizinga BJ, Strapoc D, Callaghan AV (2012) Field and laboratory studies on the bioconversion of coal to methane in the San Juan Basin. FEMS Microbiol Ecol 81(1):26–42. https://doi.org/10.1111/j.1574-6941.2011.01272.x
Wei M, Yu ZS, Jiang Z, Zhang HX (2014) Microbial diversity and biogenic methane potential of a thermogenic-gas coal mine. Int J Coal Geol 134:96–107. https://doi.org/10.1016/j.coal.2014.09.008
Zhang J, Liang YN (2017) Evaluating approaches for sustaining methane production from coal through biogasification. Fuel 202:233–240. https://doi.org/10.1016/j.fuel.2017.04.037
Zhang J, Liang YN, Pandey R, Harpalani S (2015a) Characterizing microbial communities dedicated for conversion of coal to methane in situ and ex situ. Int J Coal Geol 146:145–154. https://doi.org/10.1016/j.coal.2015.05.001
Zhang J, Liang YN, Yau PM, Pandey R, Harpalani S (2015b) A metaproteomic approach for identifying proteins in anaerobic bioreactors converting coal to methane. Int J Coal Geol 146:91–103. https://doi.org/10.1016/j.coal.2015.05.006
Zhang J, Liang YN, Harpalani S (2016a) Optimization of methane production from bituminous coal through biogasification. Appl

Energy 183:31–42. https://doi.org/10.1016/j.apenergy.2016.08.153

Zhang J, Park SY, Liang YN, Harpalani S (2016b) Finding cost-effective nutrient solutions and evaluating environmental conditions for biogasifying bituminous coal to methane ex situ. Appl Energy 165:559–568. https://doi.org/10.1016/j.apenergy.2015.12.067

Zhang R, Liu SM, Bahadur J, Elsworth D, Wang Y, Hu GL, Liang YN (2017) Changes in pore structure of coal caused by coal-to-gas bioconversion. Sci Rep 7:3840. https://doi.org/10.1038/s41598-017-04110-z

Zhang J, Anderson K, Britt D, Liang YN (2018a) Sustaining biogenic methane release from Illinois coal in a fermentor for one year. Fuel 227:27–34. https://doi.org/10.1016/j.fuel.2018.04.061

Zhang J, Bi ZT, Liang YN (2018b) Development of a nutrient recipe for enhancing methane release from coal in the Illinois basin. Int J Coal Geol 187:11–19. https://doi.org/10.1016/j.coal.2018.01.001

Publisher's Note Springer Nature remains neutral with regard to jurisdictional claims in published maps and institutional affiliations.